Journal of Colloid and Interface Science 418 (2014) 178–184

Contents lists available at ScienceDirect

Journal of Colloid and Interface Science

www.elsevier.com/locate/jcis

Molecular dynamics simulations of silver nanocluster supported on carbon nanotube

Hamed Akbarzadeh *, Hamzeh Yaghoubi

Department of Chemistry, Hakim Sabzevari University, Sabzevar, Iran

ARTICLE INFO

Article history:
Received 29 July 2013
Accepted 3 December 2013
Available online 11 December 2013

Keywords:
Molecular dynamics simulation
Silver nanoclusters
Nanotube-supported
Surface melting

ABSTRACT

We carried out molecular dynamics simulations to examine the thermal, structural and dynamics properties of single walled carbon nanotube-supported silver nanoclusters with $N = 38$, 108 and 256 atoms. The nanoclusters were simulated in two stages: first heated in 100–1700 K temperature range with steps of 100 K, then cooled to 100 K with the same steps. The number of Ag atoms in nanocluster layer in contact with the nanotube surface, the height of nanocluster and diameter of the lowest layer (layer in contact with nanotube) were calculated as a function of time. Also, the hysteresis in potential curves, surface melting, irreversibility of structural change with temperature, broaden interface structure and surface wetting were identified by analyzing the obtained data from simulations.

1. Introduction

Due to large surface atom fractions and nanoscale sizes, nanoclusters exhibit distinguishing optical, mechanical, electronic and thermal properties compared to bulk systems. For example silver nanoparticles can be applied in various widespread bases such as optical sensors [1], biosensor materials [2], cryogenic superconducting materials [3], antibacterial applications [4] and as additives in composite fibers [5]. Meanwhile, the special electrical, chemical, and mechanical characters [6] made carbon nanotubes widely used in the construction of chemical sensors and biosensors especially in the field of supporting materials [7]. The high surface area of carbon nanotubes made it possible to load nanoparticles to enhance their properties [7,8]. Ag nanoparticles deposited on carbon nanotube, have gained more industrial applications such as heterogeneous catalysis, sensors, and microelectronics [9–12]. The thermal properties of nanoclusters have been studied by various thermodynamic models [13–15] and molecular dynamics (MD) simulations [16–18]. Melting behavior and thermodynamics properties of free silver nanoclusters have been investigated and found that the melting point of nanoclusters decreases with decreasing cluster size [13,19,20]. Also, freezing structures of free silver nanodroplets containing different number of atoms have been studied by using MD simulation by Tian et al. [21]. They have observed first order and continuous phase transitions and some very interesting novelty morphologies, such as decahedral and icosahedral nanoparticles. Size dependencies of the Kauzmann temperature (T_K) and melting temperature (T_m), and size and temperature dependencies of melting enthalpy (H_m) and melting entropy (S_m) for silver nanoparticles have been obtained via MD simulation [22]. The behaviors of silver clusters with magic numbers of atoms in the 0–1300 K temperature range have been studied for the embedded atom model by the molecular dynamics method [23].

The catalytic properties of a metal cluster are modified substantially by anchoring it to support surfaces [24]. The thermal, structural and dynamic properties of metallic clusters supported on surfaces have also attracted much attention lately [25–36]. Lamas et al. performed a MD simulation to investigate the effect of inert gas adsorbates (Ar, Xe, and He) on the shape and structure of Pt nanoclusters supported on a graphite substrate. They found that the gas phase substantially alters the vacuum cluster structure, and the changes are mostly irreversible in the time frame of the simulations (2 ns), especially at temperatures well below the cluster melting point [37]. Also, Ding et al. investigated the structural and dynamic changes during melting of free and supported iron clusters ranging from 150 to 10,000 atoms. Their results revealed a method for determining effective diameters of supported metal clusters, so that the melting point dependence on cluster size can be predicted in a physically meaningful way by the same analytic model used for free clusters [14]. As the cluster size increases, a smaller fraction of atoms are on the surface of the cluster. As surface atoms have less binding energy compared to bulk atoms, therefore with increase in the number of particles, the cohesive energy is increased and a more stable structure is resulted. So, the melting point increases with increasing size. Several experiments clearly indicate that quantum behavior of metal nanoclusters is observable, and is most strongly expressed between 1 and 2 nm. Hence, particles in that size region should be

* Corresponding author. Fax: +98 571 4003323.
E-mail address: akbarzadehhamed@yahoo.com (H. Akbarzadeh).

0021-9797/$ - see front matter © 2013 Elsevier Inc. All rights reserved.
http://dx.doi.org/10.1016/j.jcis.2013.12.006

of most interest [38]. Similar studies have been performed on free and supported metallic nanoclusters [39,40].

In this paper we have simulated the heating and cooling processes on carbon nanotube-supported silver nanoclusters with 38–256 atoms (1–2 nm) in the range of 100–1700 K. We investigated the melting and freezing behavior (thermal properties), the effect of nanotube on structure of silver nanocluster (structural properties), time evolution of the number of Ag atoms in the layer in contact with substrate and dynamical properties. Because of this, we employed potential energy, heat capacity, deformation parameters, radial distribution function (RDF), Lindemann index and mean square displacement (MSD).

2. Methodology

Three FCC silver nanoclusters containing 38, 108 and 256 atoms were created by DL_POLY 2.18 program [41]. Then these clusters were placed with initial distance of 3 Å above a carbon nanotube (CNT) of only one atom thick wall. This CNT includes 800 atoms and dimensions of 15.64 Å diameter and 40.31 Å in length. (The parameter (n, m) of the carbon nanotube is (20,0).) The cell dimensions were $40.31 \times 40.31 \times 100.34$ Å^3, and periodic boundary conditions were added along the axis of CNT (The vacuum thickness is almost 85 Å). The MD simulations were carried out in canonical ensemble (*NVT*). To keep temperature constant, the Berendsen thermostat [42] with a relaxation time of 0.01 ps was applied. The equations of motion were integrated using the Verlet leapfrog algorithm [43] with a time step of 1 fs. Initially, all systems were heated in the 100–1700 K temperature range with steps of 100 K. Near the melting point, the temperature increments were reduced to 20 K. After the heating process, systems were cooled down to the initial temperature in the same steps. The simulations were carried out for 800 ps of equilibration followed by a production time of 2 ns for generating time-averaged properties.

To successfully predict the properties of FCC silver nanoclusters we used the many body quantum Sutton-Chen potential [44,45] for Ag–Ag interactions. For the Ag–C interactions we have used the Lennard–Jones potential with $\varepsilon = 0.0301$ eV and $\sigma = 3.006$ Å, which were obtained from Ag–Ag and C–C parameters [46], utilizing the geometric mean (Eq. (1)) for ε and the arithmetic mean (Eq. (2)) for σ [47].

$$\varepsilon_{Ag-C} = \sqrt{\varepsilon_{Ag-Ag} \times \varepsilon_{C-C}} \tag{1}$$

$$\sigma_{Ag-C} = \frac{\sigma_{Ag-Ag} \times \sigma_{C-C}}{2} \tag{2}$$

In these simulations, we considered two different force field models for the CNT substrate:

(1) The carbon atoms of CNT were fixed in their positions (indeed we have a static surface).
(2) The optimized Tersoff potential [48] was applied for C–C interactions of CNT. The parameters of optimized Tersoff potential for CNT can be found in Lindsay study [48].

We compared the results obtained from the two models. There was no significant difference in results between the models. The reason is that the carbon support is a "bulk" extended surface which will not be affected by the presence of the nanoclusters. We also ran several simulations considering different CNTs in terms of n, m ((20,20), (10,0), (6,4)) for the Ag_{256} nanocluster; the results were almost similar to the first CNT system. Therefore, in this paper, we have reported the results obtained from the first model. The analysis of simulated trajectories and calculation of different properties were performed using the utilities of DL_POLY 2.18 program. Fig. 1 shows the atomic structures of the carbon nanotube-supported Ag_{256} nanoclusters at important stages, such as the initial structure (a), at 300 K in heating process (b), at 500 K in heating process or surface melting (c), at 900 K in heating

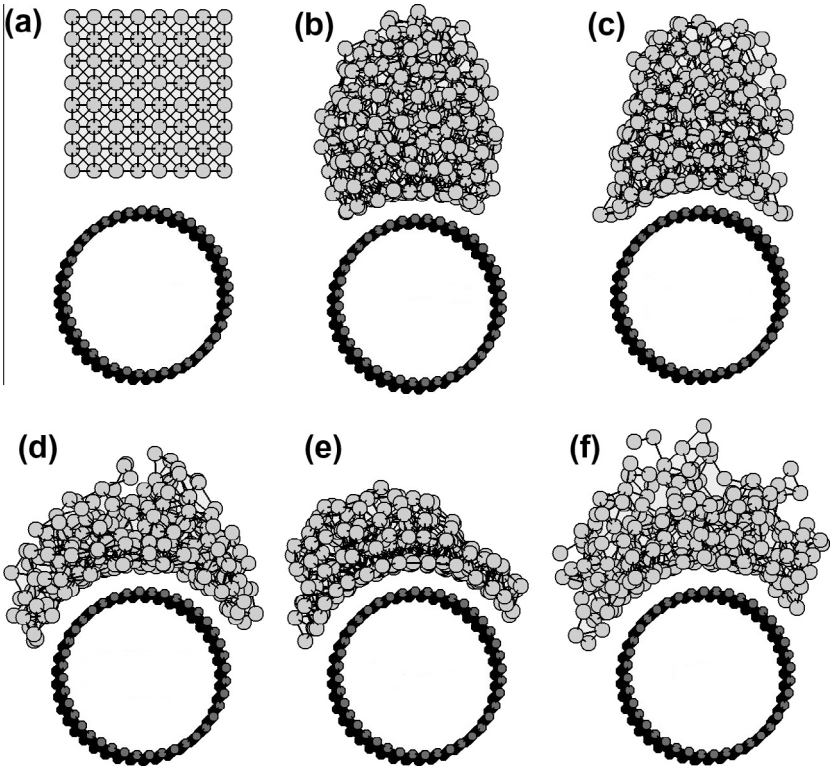

Fig. 1. The atomic structures of the carbon nanotube-supported Ag_{256} nanoclusters at important stages: the initial structure (a), at 300 K in heating process (b), at 500 K in heating process or surface melting (c), at 900 K in heating process (after melting) (d), at 300 K in cooling process (e) and at 1700 K (f).

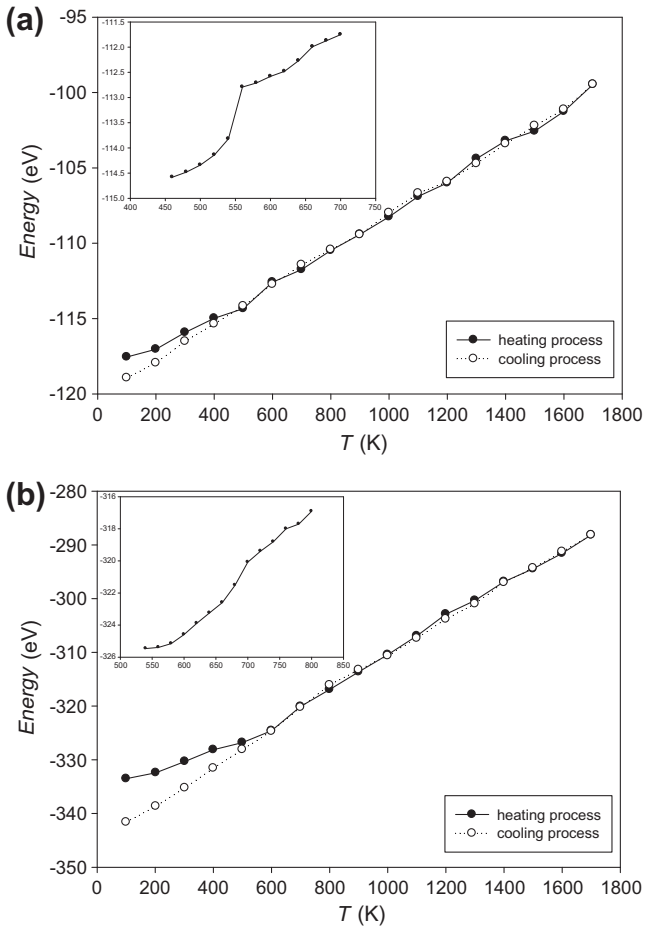

Fig. 2. The caloric curves at different temperatures for heating and cooling processes for: Ag_{38} (a), and Ag_{108} (b).

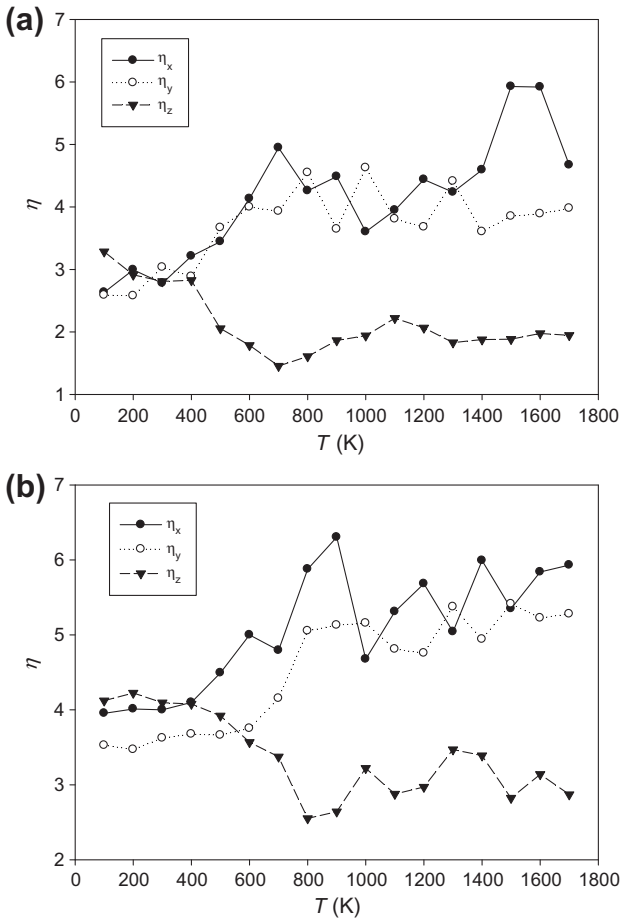

Fig. 4. The deformation parameters of Ag_{108} (a), and Ag_{256} (b) at different temperatures.

process (after melting) (d), at 300 K in cooling process (e) and at 1700 K (f).

3. Results and discussion

Potential energies versus temperature for Ag_{38} and Ag_{108} in heating process have been plotted in Fig. 2. As it is shown by the curves, simple jump can be identified, that shows the temperature range of first order phase transition. Several simulations were performed close to melting points of clusters with increment of 20 K and their potential curves have been plotted (inset in Fig. 2). Paying attention to these potential curves we recognized the melting points exactly. These curves show the sharp slope in 540–560, 660–700 and 820–840 K for $N = 38$, 108 and 256, respectively.

Also, Fig. 2 shows the cooling process potential energy versus temperature. It shows a hysteresis in the course of the cooling process (because of the existence of large difference in heating and cooling curves below the melting point temperatures). The hysteresis manifests itself in state transitions when melting temperature and freezing temperature do not agree. This means that after heating and then cooling, the nanoclusters get to a more stable state with lower energy. In this state the nanoclusters wet the nanotube surface and expand in the interface structure. It seems that the nanoclusters and the nanotube make a coherent interface structure with more stability. Also, results show that the hysteresis

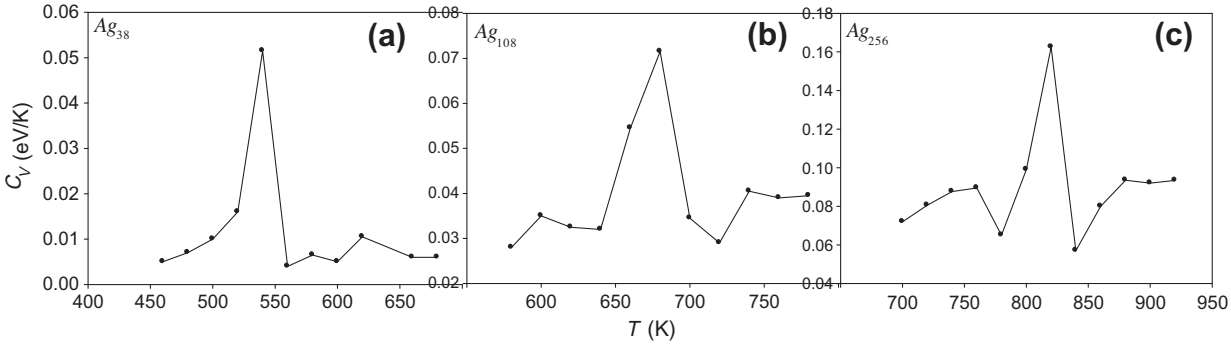

Fig. 3. The heat capacity of Ag_{38} (a), Ag_{108} (b) and Ag_{256} (c) at different temperatures.

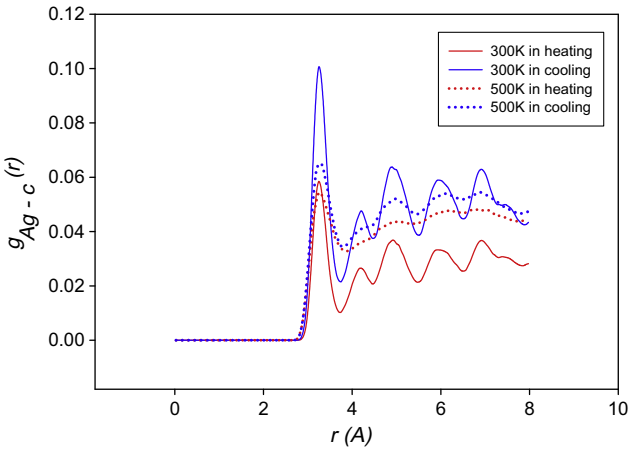

Fig. 5. RDF plots for Ag_{256}–C in 300 K (solid lines) and 500 K (dotted lines). Red color is for heating and blue color for cooling. (For interpretation of the references to color in this figure legend, the reader is referred to the web version of this article.)

decreases when the cluster size decreases. As the nanocluster with 256 atoms can make a larger interface structure, we can observe that the difference between heating and cooling curves increases with size. Similar results were obtained by Mottet and Goniakowski [49].

To specify the melting point with more accuracy, we calculated the specific heat capacity at constant volume C_v in the range of that the systems were heated with steps of 20 K. The heat capacity versus temperature for nanoclusters has been plotted in Fig. 3. The first order phase transition can be identified, that occurs in 540, 680 and 820 K for nanoclusters with 38, 108 and 256 atoms, respectively. Results show that melting temperatures are higher than that of free Ag nanoclusters of similar size and structure. Also, the melting and freezing process of free Ag nanoclusters with 38, 108 and 256 atoms were simulated. The melting temperatures for the free Ag nanoclusters are lower than that for the supported Ag nanoclusters with similar size and structure. There are two types of surface atoms for the supported Ag nanoclusters: (a) the surface atoms that are not on the substrate (free surface atoms) and (b) the surface atoms that are in contact with the substrate. The surface atoms that are in contact with the substrate have higher binding energies, compared to the free surface atoms, therefore the cohesive energy is increased and a more stable structure is resulted. But in the free nanoclusters, all of the surface atoms are free. So, the melting point of supported Ag nanoclusters is higher than that of the free Ag nanoclusters with similar size and structure.

To investigate the structural changes, we used deformation parameters that were obtained from Eq. (7):

$$\eta_q(t) = \frac{1}{N}\sum_{i=1}^{N}(|q_i(t) - q_{cm}(t)|) \tag{3}$$

In Eq. (7) $q_i = q_{(x,y,z)}$ is related to the coordinates of atom i, and q_{cm} is the nanocluster's center of mass position, and N is the number of atoms of cluster. η_q shows cluster deformation in the $q_{(x,y,z)}$ direction.

Fig. 4 shows the deformation parameters in three directions at different temperatures for $Ag_{108,256}$. At low temperature, nanoclusters have an almost spherical shape because $\eta_x \approx \eta_y \approx \eta_z$. At melting temperature, the fluctuation in η_q becomes larger, which is characteristic for the liquid state. In melting point η_z decreases, while η_x and η_y have larger values than below the melting point. Decrease in η_z is corresponding to the cluster melting, expansion of the interface structure between cluster and substrate and wetting layer. In this state cluster has rolled up around the nanotube. Two types of different forces cause these movements. The first type of the forces arises from the nanocluster–CNT interactions and the second type from the Ag–Ag interactions in the nanocluster itself. The Ag nanocluster surface atoms were redistributed to create a nanocluster with lower energy. This redistribution changes the nanocluster–CNT interfacial contact area and so the nanocluster–CNT interaction and also changes the structural variation on the cluster surface and so the Ag–Ag interaction. The large fluctuation

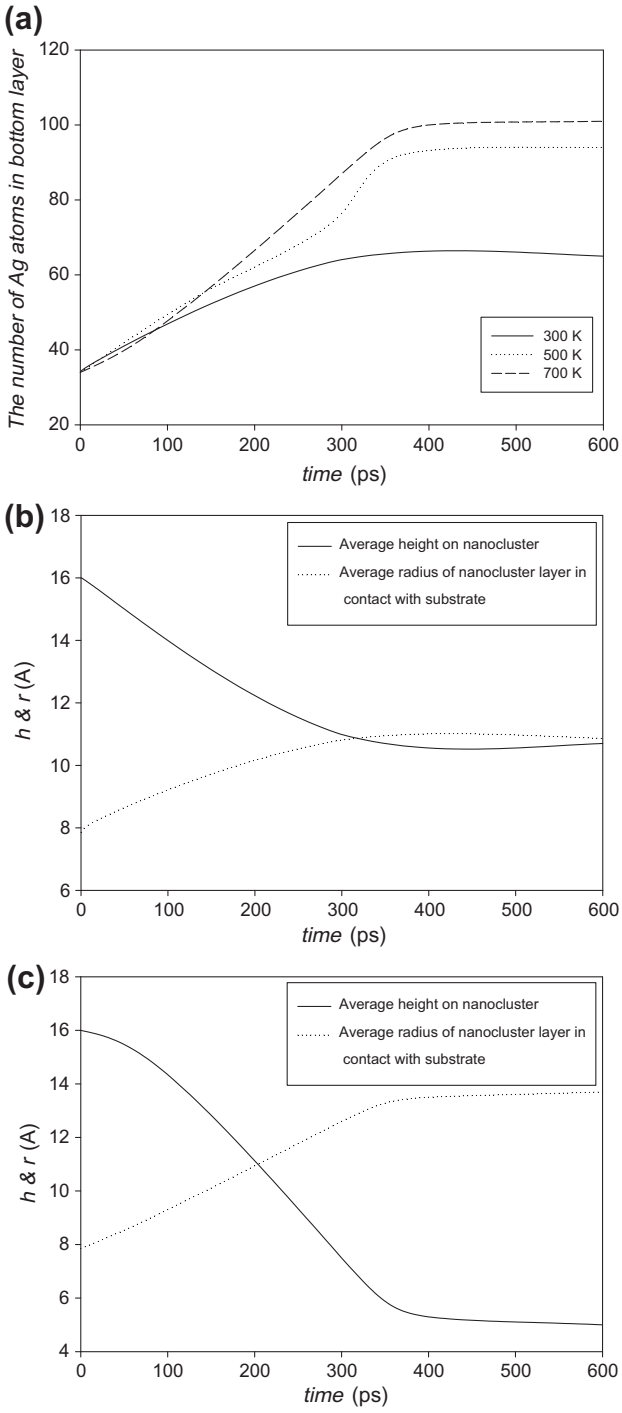

Fig. 6. Time evolution of the number of Ag atoms in the layer in contact with nanotube at 300, 500 and 700 K (a), and time evolution of nanocluster height and radius of the lowest layer at 300 K (b) and 700 K (c).

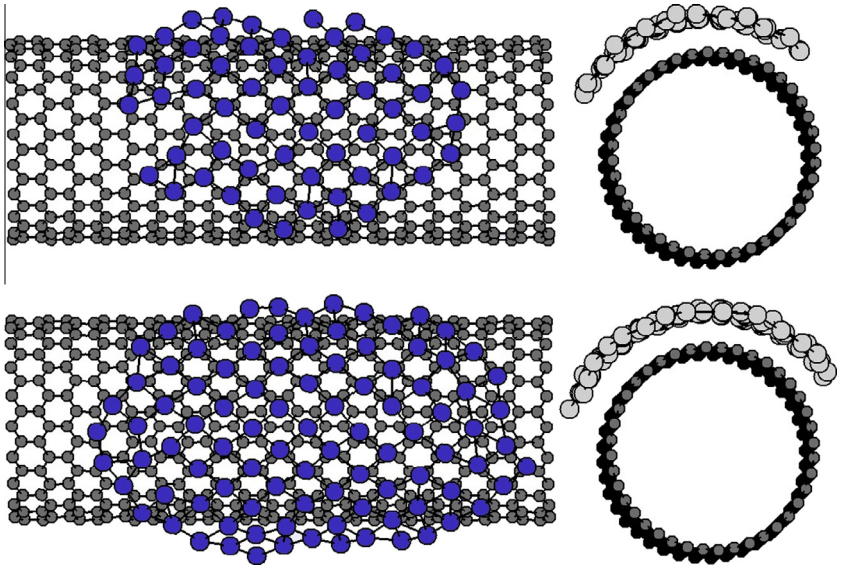

Fig. 7. The cluster layer in contact with substrate for Ag_{256} at 300 K. Top: for heating process. Bottom: for cooling process.

in η_z of Ag_{256} than Ag_{108} is related to its large size and consequently large dimension in z direction. Substantially, η_x has a larger value and fluctuation than η_y, because the length of nanotube located in x direction and the length of nanotube is almost three orders of magnitude larger than its diameter.

To examine the structural changes during the heating and cooling processes, we have used Ag–C radial distribution function (RDF). Fig. 5 shows the RDF in heating and cooling processes at 300 and 500 K (below the melting point) for Ag_{256}. In cooling curves the first peak is much larger than same peaks in heating curves, because the cluster layer in contact with nanotube has broadened and cluster has rolled up around the nanotube. By comparison the RDF curves of 300 K, well known that after melting and then freezing, the cluster layers rearrange around the nanotube.

The number of Ag atoms in nanocluster layer in contact with the nanotube surface, the height of nanocluster and diameter of the lowest layer (layer in contact with nanotube) were calculated as a function of time with steps of 30 ps. Fig. 6(a) shows the evolution of the number of Ag atoms in the lowest layer in a time period of 600 ps for Ag_{256} nanocluster at 300 K, 500 K, and 700 K. The figure illustrates that due to the increasing temperature the cluster has rolled up around the nanotube, the cluster layer in contact with substrate expands and the number of Ag atoms in lowest layer increases. Furthermore, Fig. 6(b) and (c) show the evolution of nanocluster height and radius of the lowest layer in same simulations for 300 K and 700 K, respectively. Corresponding to Fig. 6(a), as the nanocluster broadens on the nanotube; its height decreases, whereas the radius of the lowest layer increases. It can be known that the Ag_{256} nanocluster at 300 K has an almost spherical shape, instead at 700 K has a kennel shape owing to being rolled up around the nanotube.

In Fig. 7 the cluster layer in contact with nanotube at 300 K has been monitored for heating and cooling processes (The inferior division of nanotube has been deleted for clarity). It can be observed that the contact layer in cooling process has a larger area than the other.

Paying attention to Fig. 7, it can be observed that the silver atoms are located at middle of aromatic rings. (This is noticeable that owing to the curvature of nanotube in this case they can be observed by looking in the normal direction to the nanotube surface); because of this state the silver and carbon atoms have maximum interaction. Also the surface wetting occurs and cluster reaches to a more stable state and the structural change with temperature is irreversible.

To examine the dynamics of Ag nanoclusters, we investigated the MSD and self-diffusion coefficient (D). So, mean square displacement (MSD) of nanoclusters was calculated by Eq. (4):

$$\mathrm{MSD}(t) = \frac{1}{N}\sum_{i=1}^{N}(|r_i(t+\Delta t) - r_i(t)|)^2 \tag{4}$$

where $r_i(t)$ is vector position of the atom i at time t, and N is the number of atoms of cluster. And the self-diffusion coefficient was calculated by Eq. (5):

$$D = \frac{1}{6}\lim_{t\to\infty}\frac{d(MSD)}{dt} \tag{5}$$

Fig. 8 shows the value of the self-diffusion coefficient at different temperatures. At low temperature, the nanocluster has a solid structure, characterized by its constant and near the zero values of D. At melting temperature the value of the D increases suddenly that shows the liquid phase. The mild slope in the curve D relates to the surface melting that is below the melting point.

Fig. 9 shows the MSD of Ag_{256} nanocluster at 300 K in heating and cooling processes. Our calculations indicate that the cluster

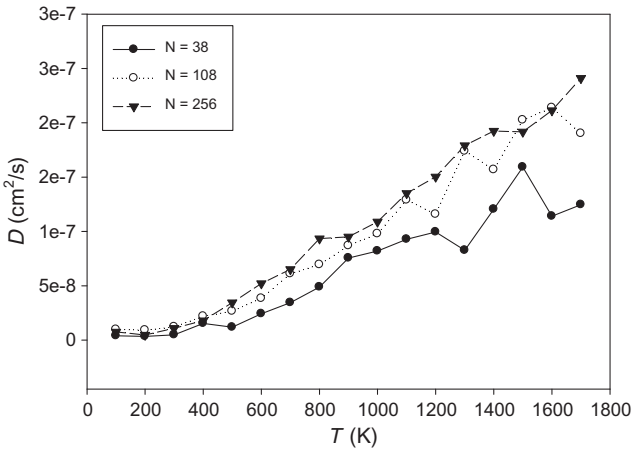

Fig. 8. Self-diffusion coefficient for silver nanocluster at different temperatures.

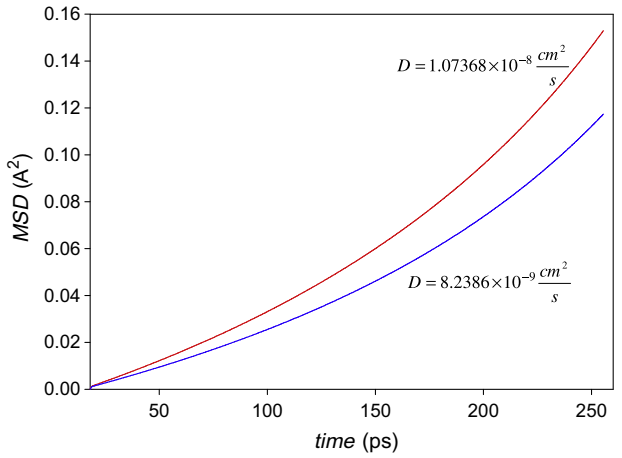

Fig. 9. MSD of cluster with 256 atoms at 300 K in heating (red line) and cooling (blue line) processes. (For interpretation of the references to color in this figure legend, the reader is referred to the web version of this article.)

mobility on substrate is low at cluster solid phase, due to the coherent interface structure. Also, identified that the cluster mobility at temperature below the melting point in cooling process is a few lower than heating process. It seems that it is due to the larger cluster layer in contact with substrate at cooling process than the other. Comparison of the MSD and diffusivity of silver cluster at 300 K for heating and cooling processes shows that the MSD and diffusivity of cluster at temperature below the melting point for cooling processes is a few minor than heating processes, owing to the expansion of cluster on nanotube.

Also, we have calculated the Lindemann index of each atom [50]

$$\delta_i = \frac{1}{N-1}\sum_{j(\neq i)} \frac{\sqrt{\langle r_{ij}^2\rangle_\tau - \langle r_{ij}\rangle_\tau^2}}{\langle r_{ij}\rangle} \tag{6}$$

where δ_i is the Lindemann index of the ith atom, $<>_T$ denotes the thermal average at temperature T and r_{ij} is the separation of atoms i and j.

Fig. 10 shows the Lindemann indices of atoms in the supported Ag_{256} nanocluster as a function of their distance from the cluster center of mass. The nanocluster is at 200 K and 800 K (which is slightly below the melting point). This figure states that the nanocluster rolls up around the nanotube at 800 K. At 800 K, the surface

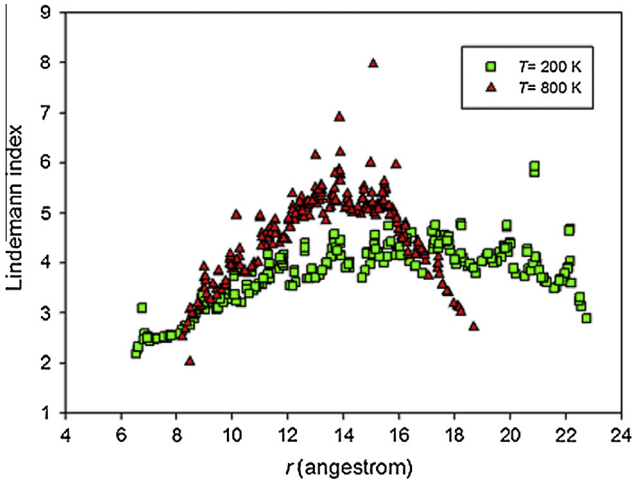

Fig. 10. Lindemann indices for the supported Ag_{256} nanocluster at 200 K and 800 K.

atoms that are not on the substrate form a liquid-like layer. However, the atoms that are in contact with the substrate are not mobile since they are stabilized by the cluster–substrate interaction. The surface of the supported cluster is thus nonhomogenous with high and low mobility regions. However, at 200 K, the surface atoms that are not on the substrate do not form a liquid layer. Therefore, the fluctuations of the Lindemann index are less at 200 K.

4. Conclusions

Using molecular dynamics simulations, we investigated the thermal, structural and dynamic properties of carbon nanotube-supported Ag nanoclusters during melting and freezing processes. By analyzing the potential energy, heat capacity, deformation parameter, self-diffusion coefficient, Lindemann index, and so on, the melting points and stable structures were got for Ag nanoclusters on carbon nanotube. It was found that the melting point of Ag nanoclusters was simulated in the range of 100–1700 K, depending on the atom numbers and contact positions on the nanotube. The mobility and diffusivity of Ag atoms at temperatures below the melting points in the cooling process are slower than the ones in the heating process. Also, the results show that at temperatures above the melting point, the cluster was flattened on substrate and rolled up around the nanotube and surface wetting occurred.

References

[1] A. Michaels, J. Jiang, L. Brus, J. Phys. Chem. B 104 (2000) (1971) 11965–11971.
[2] X.L. Ren, F.Q. Tang, Acta Chim. Sin. 60 (2002) 393–397.
[3] S. Hirano, Y. Wakasa, A. Saka, S. Yoshizawa, Y. Oya-Seimiya, Y. Hishinuma, A. Nishimura, A. Matsumoto, H. Kumakura, Physica C 392 (2003) 458–462.
[4] H. Jiang, S. Manolache, A.C.L. Wong, F.S. Denes, J. Appl. Polym. Sci. 93 (2004) 1411–1422.
[5] S.Y. Yeo, H.J. Lee, S.H. Jeong, J. Mater. Sci. 38 (2003) 2143–2147.
[6] X. Zhang, Y. Ye, H. Wang, S. Yao, Radiat. Phys. Chem. 79 (2010) 1058.
[7] Y. Shi, Z. Liu, B. Zhao, Y. Sun, F. Xu, Y. Zhang, Z. Wen, H. Yang, Z. Li, J. Electroanal. Chem. 656 (2011) 29.
[8] J.H. Lee, N.R. Kim, B.J. Kim, Y.C. Joo, Carbon 50 (2012) 98.
[9] Q. Zhao, M. Buongiorno, Nano Lett. 5 (2005) 847.
[10] S. Sahoo, S. Husale, S. Karna, S.K. Nayak, P.M. Ajayan, J. Am. Chem. Soc. 133 (2011) 4005.
[11] Z.D. Lin, S.J. Young, C.H. Hsiao, S.J. Chang, Sens. Actuators 188 (2013) 1230.
[12] T. Liu, H.Q. Tang, X.M. Cai, J. Zhao, D.J. Li, R. Li, X.L. Sun, Nucl. Instrum. Methods B 264 (2007) 282.
[13] K.K. Nanda, S.N. Sahu, S.N. Behera, Phys. Rev. A 66 (2002) 013208.
[14] F. Ding, A. Rosen, Appl. Phys. Lett. 88 (2006) 133110.
[15] M. Wautelet, Phys. Lett. A 246 (1998) 341.
[16] S.K.R.S. Sankaranarayanan, V.R. Bhethanabotla, B. Joseph, Phys. Rev. B 76 (2007) 134117.
[17] H. Akbarzadeh, G. Parsafar, Fluid Phase Equilib. 280 (2009) 16.
[18] Y. Qi, T. Cagin, W.L. Johnson, W.A. Goddard, J. Chem. Phys. 115 (2001) 385.
[19] C.C. Yang, S. Li, Phys Rev. B 75 (2007) 165413.
[20] W.H. Luo, W.Y. Hu, S.F. Xiao, J. Phys. Chem. C 112 (2008) 2359.
[21] Z.-A. Tian, R.-S. Liu, P. Peng, Z.-Y. Hou, H.-R. Li, C.-X. Zheng, K.-J. Dong, A.-B. Yu, Phys. Lett. A 373 (2009) 1667–1671.
[22] Z.M. Ao, W.T. Zheng, Q. Jiang, Nanotechnology 18 (2007) 255706.
[23] V.I. Kuzmin, D.L. Tytik, D.K. Belashchenko, A.N. Sirenko, Colloid J. 70 (2008) 284–296.
[24] C.F. Sanz-Navarro, P. Åstrand, D. Chen, M. Rønning, A.C.T. vanDuin, W.A. Goddard III, J. Phys. Chem. C 114 (2010) 3522.
[25] D. Bazin, Top. Catal. 18 (2002) 79.
[26] S.-P. Huang, D.S. Mainardi, P.B. Balbuena, Surf. Sci. 545 (2003) 163.
[27] K. Hata, D.N. Futaba, K. Mizuno, T. Namai, M. Yumura, S. Lijima, Science 306 (2004) 1362.
[28] A. Moisala, A.G. Nasibulin, E.I. Kauppinen, J. Phys.: Condens. Matter 15 (2003) S3011.
[29] F. Ding, K. Bolton, A. Rosen, J. Phys. Chem. B 108 (2004) 17369.
[30] A.R. Harutyunyan, T. Tokune, E. Mora, Appl. Phys. Lett. 87 (2005) 051919.
[31] S. Jalili, C. Mochani, M. Akhavan, J. Schofield, Mol. Phys. 110 (2012) 267.
[32] S.-P. Huang, P.B. Balbuena, Mol. Phys. 100 (2002) 2165.
[33] P. Jensen, A. Clement, L.J. Lewis, Comput. Mater. Sci. 30 (2004) 137.
[34] J.C. Jimenez-Saez, A.M.C. Perez-Martin, J.J. Jimenez-Rodrıguez, Nucl. Instrum. Methods B 249 (2006) 816.
[35] C.F. Sanz-Navarro, P.-O. Astrand, D. Chen, M. Rønning, A.C.T. van Duin, J.E. Mueller, W.A. Goddard III, J. Phys. Chem. C 112 (2008) 12663.
[36] Y. Shibuta, S. Maruyama, Chem. Phys. Lett. 437 (2007) 218.

[37] E.J. Lamas, P.B. Balbuena, J. Phys. Chem. B 107 (2003) 11682.
[38] G. Schmid, M. Baumle, M. Geerkens, I. Helm, C. Osemann, T. Sawitowski, Chem. Soc. Rev. 28 (1999) 3.
[39] S.K.R.S. Sankaranarayanan, V.R. Bhethanabotla, B. Joseph, Phys. Rev. B 72 (2005) 195405.
[40] S.H. Lee, S.S. Han, J.K. Kang, J.H. Ryu, H.M. Lee, Surf. Sci. 602 (2008) 1433–1439.
[41] W. Smith, I.T. Todorov, Mol. Simul. 32 (2006) 935.
[42] H.J.C. Berendsen, J.P.M. Postma, W.F. Gunsteren, A. Dinola, J.R. Haak, J. Chem. Phys. 81 (1984) 3684.
[43] M.P. Allen, D.J. Tildesley, Computer Simulation of Liquid, Clarendon, Oxford, 1997.
[44] A.P. Sutton, J. Chen, Philos. Mag. Lett. 61 (1990) 139.
[45] Y. Qi, T. Cagin, Y. Kimura, W.A. Goddard III, Phys. Rev. B 59 (1999) 3527.
[46] M. Neek-Amal, R. Asgari, M.R. Rahimi Tabar, Nanotechnology 20 (2009) 135602.
[47] A. Steel, The Introduction of Gases with Solid Surface, Oxford, Pergamon, 1974.
[48] L. Lindsay, D.A. Broido, Phys. Rev. B 81 (2010) 205441.
[49] C. Mottet, J. Goniakowski, Surf. Sci. 566–568 (2004) 443–450.
[50] F.A. Lindemann, Phys. Z. 11 (1910) 609.